

# Observation of the quantized motion of excitons in CdSe nanoplatelets

Michele Failla<sup>1</sup>, Francisco García Flórez<sup>2</sup>, Bastiaan B. V. Salzmann<sup>3</sup>, Daniel Vanmaekelbergh<sup>3</sup>, Henk T. C. Stoof<sup>2</sup>, and Laurens D. A. Siebbeles<sup>1</sup>

<sup>1</sup>*Chemical Engineering Department, Delft University of Technology, Van der Maasweg 9, NL-2629 HZ Delft, The Netherlands*

<sup>2</sup>*Institute for Theoretical Physics and Center for Extreme Matter and Emergent Phenomena, Utrecht University, Princetonplein 5, 3584 CC Utrecht, The Netherlands*

<sup>3</sup>*Debye Institute, Condensed Matter and Interfaces, Utrecht University, P.O. Box 80.000, 3508 TA Utrecht, The Netherlands*



(Received 17 July 2020; revised 11 September 2020; accepted 12 October 2020; published 4 November 2020)

We show that the finite lateral sizes of ultrathin CdSe nanoplatelets strongly affect both their photoluminescence and optical absorption spectra. This is in contrast to the situation in quantum wells, in which the large lateral sizes may be assumed to be infinite. The lateral sizes of the nanoplatelets are varied over a range of a few to tens of nanometers. For these sizes excitons experience in-plane quantum confinement, and their center-of-mass motion becomes quantized. Our direct experimental observation of the discretization of the exciton center-of-mass states can be well understood on the basis of the simple particle-in-a-box model.

DOI: [10.1103/PhysRevB.102.195405](https://doi.org/10.1103/PhysRevB.102.195405)

## I. INTRODUCTION

Cadmium selenide nanoplatelets (CdSe NPLs) are solution-processable two-dimensional (2D) semiconductor nanomaterials which are grown with an atomically precise thickness [1,2] [see Figs. 1(a) and 1(b)]. They receive considerable attention due to promising optical properties for optoelectronic applications, including strong optical oscillator strength [3], large exciton binding energy [3–5], weak exciton-phonon coupling [4], high photoluminescence (PL) quantum yield [6], efficient two-photon absorption [7–9], and lasing [7,10,11].

The steady-state optical absorption spectrum exhibits well-resolved peaks due to the formation of heavy-hole (HH) and light-hole (LH) excitons [see Fig. 1(c)]. The energy at which the HH and LH peaks appear in the optical absorption spectrum, as well as the PL energy, strongly depend on the NPL thickness,  $L_z$  in Fig. 1(a), which is of the order of a nanometer [1,12]. Hence, in a NPL excitons are strongly quantum confined along this (vertical) direction.

Besides the atomically precise thickness, the lateral sizes of CdSe NPLs,  $L_x$  and  $L_y$  in Fig. 1(a), can also be tuned from a few to tens of nanometers by varying the synthesis procedure [13]. The strong vertical and weak, intermediate, or strong in-plane quantum confinement regimes [14,15] cause the optical properties of NPLs to be in between those of quantum wells (with lateral sizes exceeding microns or larger) and quantum dots. Experimentally, reducing the lateral sizes of CdSe NPLs has been reported to blueshift and narrow the optical absorption and PL peaks [12,13,16], decrease the absorption cross section [17], and affect the optical gain and amplified spontaneous emission [17–21].

An interesting peculiarity, commonly observed in the absorption spectrum of CdSe NPLs, is the asymmetric shape of the HH exciton peak, which exhibits a tail on the side of higher

photon energy [see Fig. 1(c)], whose explanation has been inconclusive. It has, for instance, been ascribed to fluctuations in the confining potential of NPLs that lead to localization and, consequently, an increased energy of the excitons [3,5,10,22] or to internally excited exciton states [23,24]. As depicted in Fig. 1(a), excitons have a Bohr radius much smaller than the lateral dimensions of a NPL. Hence, the center-of-mass (c.m.) translational motion in the plane of a NPL must also be considered, and photoexcitation to c.m. motional states with nonzero in-plane momentum can, indeed, give rise to the high-energy tail of the HH exciton peak. Until now, however, this c.m. motion of an exciton has not yet been invoked to explain the PL and absorption spectra. The finite lateral size of NPLs then also affects the c.m. energy of excitons, as discussed by Richter [15]. The presence of these states has also been invoked to explain the exciton dynamics probed by transient resonant four-wave mixing [3] and transient PL spectra at temperatures below 200 K [25,26]. The latter exhibits two PL peaks with a lateral size-dependent energy difference of tens of meV. Nonetheless, these PL peaks have also been explained by considering phonon replicas [27].

In this paper, we directly observe the discretized center-of-mass states of excitons from the lateral size dependence of experimental PL and optical absorption spectra of CdSe NPLs. Both spectra are simultaneously interpreted and accurately modeled by considering the in-plane c.m. motion of excitons. In particular, quantum effects of spatial lateral confinement explain the size dependence of both the PL and absorption peak positions and widths. Our work provides an explanation of the hitherto open problem of understanding the effects of lateral size of NPLs on the properties of excitons. It can now be understood how variation of the lateral size of (quasi-)two-dimensional materials provides a tool to continuously tune their optical properties in addition to the discrete changes by adjustment of the thickness.

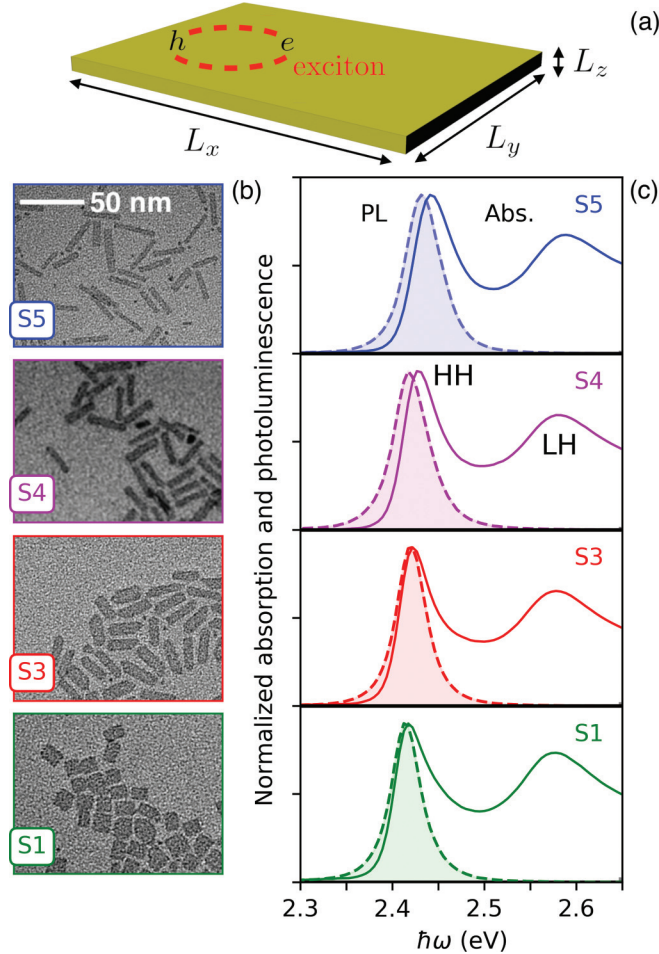


FIG. 1. (a) Scheme of a nanoplatelet. The exciton center-of-mass motion is influenced by the lateral sizes  $L_x$  and  $L_y$ . (b) TEM images of the investigated CdSe NPLs. (c) Photoluminescence (dashed lines) and optical absorption (solid lines) spectra for samples in (b). The absorption peaks at low and high energies are due to HH and LH excitons, respectively.

## II. LATERAL SIZES

Four samples of CdSe NPLs with a thickness of 4.5 monolayers ( $L_z \simeq 1.4$  nm [4]) and different average lateral sizes were synthesized by following Ref. [13] (see Supplemental Material, Sec. I [28]). The average lateral sizes ( $L_x^{\text{avg}}$ ,  $L_y^{\text{avg}}$ ) were determined from transmission electron microscopy (TEM) images, as shown in Fig. 1(b), by assuming a Gaussian size distribution (see Fig. SM1 in the Supplemental Material [28]). The results are shown in Table I, together with the NPL areas and aspect ratios  $r_l \equiv L_x^{\text{avg}}/L_y^{\text{avg}}$ . The samples are labeled based on their aspect ratio (first column in Table I). The data presented in this work are obtained from PL and optical absorption ensemble measurements on NPLs dispersed in hexane.

## III. EXCITON CENTER-OF-MASS ENERGY

Figure 1(c) shows the dependence of PL (dashed lines) and absorption spectra (solid lines) on the NPL size. Spectra are normalized for comparison. Two clearly distinguishable

TABLE I. Average lateral sizes ( $L_x^{\text{avg}}$ ,  $L_y^{\text{avg}}$ ), area, and aspect ratio  $r_l$  of the CdSe NPL samples. Samples are labeled based on their aspect ratio.

Sample	$L_x^{\text{avg}}$ (nm)	$L_y^{\text{avg}}$ (nm)	Area (nm <sup>2</sup> )	$r_l$
S5	$29.3 \pm 3.3$	$5.4 \pm 0.8$	159	5.4
S4	$26.1 \pm 3.3$	$6.4 \pm 1.1$	167	4.1
S3	$25.4 \pm 2.9$	$8.1 \pm 0.9$	204	3.2
S1	$13.7 \pm 2.2$	$13.4 \pm 1.9$	183	1.0

absorption peaks are related to HH and LH exciton states. In agreement with Refs. [13,16], by decreasing the aspect ratio, we observe (i) a redshift of all features, (ii) a decrease of the PL linewidth, (iii) a decrease of the Stokes shift, and (iv) an increase of the asymmetry (tail on the high-energy side) of the HH exciton peak. As mentioned above, observation (iv) may be related to the presence of phonon replicas [27]. However, the latter cannot be dominant since the small Stokes shifts in Fig. 1(c) imply weak exciton-phonon coupling. In addition, phonon replicas also give rise to a strong asymmetry on the low energy side of the PL peak, in contrast to the data in Fig. 1(c). We highlight that observation (iii) may be due to the environment surrounding the NPLs (i.e., solvent or defects). This must result in a bigger Stokes shift for narrower NPLs, which is what we observe.

In order to interpret and explain the observations listed above, we now consider c.m. exciton states and their change with the lateral dimensions of the NPLs. Since the NPL thickness  $L_z$  is smaller than the bulk exciton Bohr radius,  $a_B^{\text{3D}} = 5.4$  nm [16], excitons experience strong quantum confinement along the  $z$  direction [14,15,29]. This strong confinement increases the exciton binding energy and reduces the Bohr radius to a quasi-2D value,  $a_B^{\text{2D}} = 1.8\text{--}4.1$  nm [4,16,30], which is smaller than the lateral sizes of the NPLs investigated in this work. Hence, excitons in a NPL are described by approximately factorizing their perpendicular and in-plane wave functions as [14,15,31]  $\Psi(z_e, z_h, \mathbf{r}, \mathbf{R}) \simeq u_{n_z}^e(z_e)u_{n_z}^h(z_h)\psi^{\text{rel}}(\mathbf{r})\psi_{n_x, n_y}^{\text{c.m.}}(\mathbf{R})$ , where  $z_{e,h}$  are the coordinates of electrons ( $e$ ) and holes ( $h$ ) perpendicular to the plane of the NPL,  $\mathbf{r} = \mathbf{r}_e - \mathbf{r}_h$  and  $\mathbf{R} = (m_e \mathbf{r}_e + m_h \mathbf{r}_h)/(m_e + m_h)$  are the relative and c.m. coordinates in the plane of the NPL, respectively, with  $m_e$  ( $m_h$ ) being the electron (hole) effective mass, and  $m_e + m_h = M$  is the total exciton mass, while  $n_i$  are quantum numbers along the  $i$ th direction. The wave functions  $u_{n_z}^{e,h}$  give rise to a confinement energy of both the electron and the hole of  $E_z = E_{n_z=1}^e(L_z) + E_{n_z=1}^h(L_z) = \pi^2 \hbar^2 / (2\mu L_z^2)$ , where  $\mu = m_e m_h / (m_e + m_h)$  is the reduced effective mass of the  $e$ - $h$  pair. The wave function  $\psi^{\text{rel}}(\mathbf{r})$  describes the relative or internal exciton wave function, which can be obtained by using the appropriate Coulomb potential. The c.m. wave function  $\psi_{n_x, n_y}^{\text{c.m.}}(\mathbf{R})$  is obtained by using the particle-in-a-box potential, resulting in c.m. exciton states with energy

$$E_{n_x, n_y}(L_x, L_y) = \frac{\pi^2 \hbar^2}{2M} \left[ \left( \frac{n_x}{L_x} \right)^2 + \left( \frac{n_y}{L_y} \right)^2 \right]. \quad (1)$$

For convenience, in what follows we use the notation  $\mathbf{L} = (L_x, L_y)$  and  $\mathbf{n} = (n_x, n_y)$ , so that the dependence of the energy

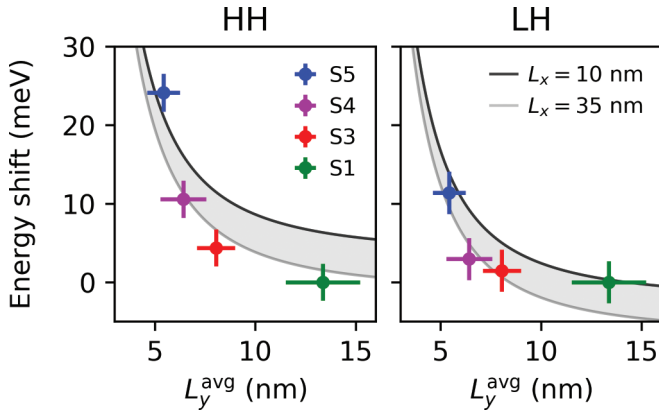


FIG. 2. Energy shift for HH (left) and LH (right) exciton absorption peaks from Fig. 1(c) as a function of the small lateral size  $L_y^{\text{avg}}$ . This shift is considered with respect to the HH and LH energies of sample S1. Shaded areas are energy ranges obtained from Eq. (1) with  $L_x$  between 10 and 35 nm.

in Eq. (1) on the lateral size and quantum number is denoted as  $E_n(L)$ .

The validity of our approach is first verified by focusing on the energy shift of the HH and LH absorption peaks as the small lateral size  $L_y$  is varied, as shown in Fig. 2. This shift is considered from the exciton peak energies (for HH and LH) of the larger NPLs (sample S1, green dots). Vertical and horizontal bars depict the indetermination of the experimental peak energies ( $\pm 0.5$  nm in our spectrometer) and  $L_y^{\text{avg}}$ , respectively, with the latter given in Table I. The shaded area represents the range of calculated energies from Eq. (1) with  $\mathbf{n} = (1, 1)$ ,  $m_e = 0.27 m_0$ , the HH mass  $m_{hh} = 0.45 m_0$ , the LH mass  $m_{lh} = 0.52 m_0$  [32], and  $L_x$  between 10 and 35 nm. The agreement between the calculated and experimental energy shift is clear evidence of the role of spatial lateral confinement on the exciton c.m. motion.

According to the particle-in-a-box model, the c.m. wave function for the in-plane motion of an exciton is given by

$$\psi_{n_x, n_y}^{\text{c.m.}}(x, y) = \sqrt{\frac{4}{L_x L_y}} \sin\left(\frac{n_x \pi x}{L_x}\right) \sin\left(\frac{n_y \pi y}{L_y}\right). \quad (2)$$

The oscillator strength for photoexcitation from the electronic ground state is nonzero only for odd values of both  $n_x$  and  $n_y$  and is proportional to [31]

$$f_n(L) = \left| \int_0^{L_x} \int_0^{L_y} dx dy \psi_{n_x, n_y}^{\text{c.m.}}(x, y) \right|^2 = \frac{64 L_x L_y}{\pi^4 n_x^2 n_y^2}. \quad (3)$$

The oscillator strength described by Eq. (3) is in line with the experimental observation of an enhanced absorption cross section for larger NPLs [17]. Moreover, the inverse-square dependence on  $\mathbf{n}$  agrees with the observed asymmetry on the high-energy side of the HH exciton absorption peak, as shown in Fig. 1(c). It is worth mentioning that this asymmetry may also arise from the presence of internally excited excitons with quantum number  $n_B > 0$ . Nevertheless, in a 2D system, their oscillator strength is expected to scale as  $(n_B + 1/2)^{-3}$  [32]. This implies that the second optically active c.m. state (1,3) for the  $n_B = 0$  exciton is 3 times stronger than the (1,1) c.m. state for the  $n_B = 1$  exciton. Therefore, in what follows, the influence of internally excited excitons states will be neglected for simplicity.

#### IV. PHOTOLUMINESCENCE SPECTRA

To model PL and absorption spectra of an ensemble of NPLs, it is essential to average over the known population distribution  $D(L)$  of CdSe NPLs in the sample, which is a Gaussian distribution reported in Fig. SM1 of the Supplemental Material [28]. PL spectra are due to photon emission from HH excitons in c.m. motional states with quantum numbers  $\mathbf{n} = (n_x, n_y)$ . This leads to the following expression for the PL intensity at photon energy  $\hbar\omega$ :

$$I_{\text{PL}}(\hbar\omega) = \sum_{\mathbf{n}} \int dL D(L) f_n(L) e^{-\hbar\omega/k_B T} \times \mathcal{V}(\hbar\omega - E^{\text{HH}} - E_n^{\text{HH}}(L); \Gamma^{\text{HH}}(\hbar\omega), \sigma^{\text{HH}}). \quad (4)$$

The exponential factor is due to the classical Maxwell-Boltzmann (MB) distribution over thermalized c.m. motional states. The broadening of each of these states is modeled by the Voigt distribution [23,25]  $\mathcal{V}(\hbar\omega - E_0; \Gamma^{\text{HH}}(\hbar\omega), \sigma^{\text{HH}})$ , centered at  $E_0 = E^{\text{HH}} + E_n^{\text{HH}}(L)$ , where  $E^{\text{HH}}$  is the exciton state with zero c.m. energy, which is determined also by the  $z$  confinement and Stokes shift. The term  $E_n^{\text{HH}}(L)$  is

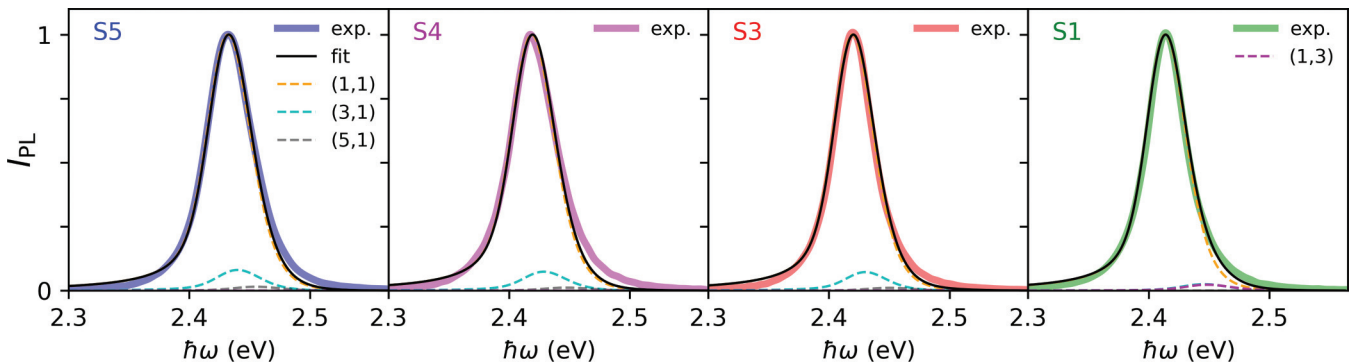


FIG. 3. Fits (black lines) of experimental photoluminescence spectra (thick colored lines) from our CdSe NPLs with different lateral sizes (see Table I). Our model considers the contribution of different exciton c.m. motional states (thin dashed colored lines), with quantum numbers  $\mathbf{n} = (n_x, n_y)$ , whose energy and oscillator strength are influenced by the size distribution [Eqs. (1) and (3)].

calculated from Eq. (1).  $\Gamma^{\text{HH}}$  and  $\sigma^{\text{HH}}$  are the linewidths of the Lorentzian and Gaussian distribution defining  $\mathcal{V}$ , respectively. The former accounts for the exciton-phonon interaction, which, according to the Urbach rule [33], is given by  $\Gamma^{\text{HH}}(\hbar\omega) = \Gamma_0^{\text{HH}} / (e^{[E^{\text{HH}} + E_n^{\text{HH}}(L) - \hbar\omega]/k_B T} + 1)$ .  $\sigma^{\text{HH}}$  is here attributed to the inhomogeneous broadening due to structural, size-independent disorder, e.g., nonflatness of NPLs, effects of surface ligands on the NPLs, or the deviation of the shape of the NPLs from perfect rectangles. The only fit parameters for modeling PL spectra from Eq. (4) for all samples are  $E^{\text{HH}}$ ,  $\Gamma_0^{\text{HH}}$ , and  $\sigma^{\text{HH}}$ .

Figure 3 shows the obtained PL fits (thin black lines), which agree well with the experimental spectra (thick colored lines) for every sample. The slight mismatch between fit and data on the high-energy side of the PL peaks is probably related to the presence of internally excited exciton states, together with their c.m. states, as mentioned above. The fits are obtained with  $\Gamma_0^{\text{HH}} = 26 \pm 1$  meV and  $\sigma^{\text{HH}} = 14 \pm 1$  meV for all samples. The contribution of different states is also depicted (dashed lines). For rectangular NPLs ( $r_l > 1$ ), besides the main PL from (1,1) states, the contribution at higher energies is due to (3,1) (magenta) and (5,1) (gray) states. The small contribution from the (5,1) states is due to the decrease of the oscillator strength with  $n$  [see Eq. (3)], as well as to the MB distribution. Due to the square shape of the NPLs in sample S1 ( $r_l = 1$ ), the (3,1) and (1,3) (cyan) states contribute with a similar oscillator strength and energy. Since  $\Gamma_0^{\text{HH}}$  and  $\sigma^{\text{HH}}$  are the same for all samples, the decreasing experimental PL linewidth, going from sample S5 to sample S1, is explained by a reduction of the effects of the lateral size distribution of the NPLs via  $D(L)$  and, in turn,  $f_n(L)$ .

## V. ABSORPTION SPECTRA

The exciton absorption is modeled similarly to the PL and is given by

$$\mathcal{A}^J(\hbar\omega) = \sum_n \int dL D(L) f_n(L) \times \mathcal{V}(\hbar\omega - E^J - E_n^J(L); \Gamma^J(\hbar\omega), \sigma^J), \quad (5)$$

where  $J = \text{HH}, \text{LH}$ . Note that the MB distribution does not appear in Eq. (5) since the initial state for absorption is the electronic ground state of a NPL. Transitions from the valence to the conduction band (continuum) also need to be taken into account and are calculated as

$$\begin{aligned} \mathcal{C}^J(\hbar\omega) &= \sum_n \int dL D(L) f_n(L) \\ &\times \int_{-\infty}^{\infty} d\epsilon_0 \mathcal{V}(\hbar\omega - \epsilon_0; \Gamma_c^J(\hbar\omega), \sigma_c^J) \\ &\times \Theta[\epsilon_0 - E_X^J - E^J - E_n^J(L)], \end{aligned} \quad (6)$$

where  $\Gamma_c^J$  and  $\sigma_c^J$  are the Lorentzian and Gaussian linewidths of the continuum, respectively,  $\Theta(x)$  is the step function [that is,  $\Theta(x) = 1$  for  $x > 0$  and zero otherwise], and  $E_X^J$  is the exciton binding energy, which is defined to be positive. By means of Eqs. (5) and (6), the absorption due to all above-mentioned

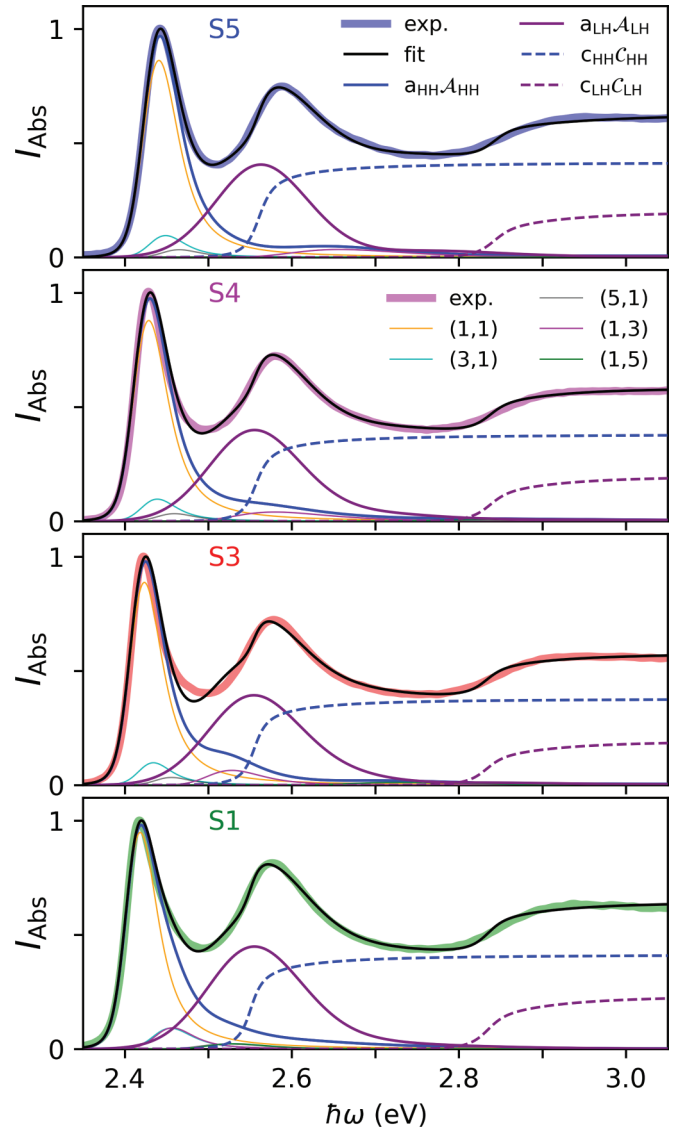


FIG. 4. Fits (black lines) of our model given by Eqs. (5), (6), and (7) to the experimental absorption spectra. The presence of exciton c.m. motional states,  $\mathbf{n} = (n_x, n_y)$  (depicted by thin colored lines), and their dependence on the lateral sizes of the NPLs explain and reproduce the change in the asymmetry on the high-energy side of the HH absorption peak.

states is

$$I_{\text{Abs}}(\hbar\omega) = a^{\text{HH}} \mathcal{A}^{\text{HH}}(\hbar\omega) + a^{\text{LH}} \mathcal{A}^{\text{LH}}(\hbar\omega) + c^{\text{HH}} \mathcal{C}^{\text{HH}}(\hbar\omega) + c^{\text{LH}} \mathcal{C}^{\text{LH}}(\hbar\omega), \quad (7)$$

where each contribution is weighted with fitted coefficients  $a^J$  and  $c^J$  that take into account the optical dipole moments involving the relative motion of electrons and holes in the exciton and continuum states, respectively. The values of  $E^{\text{HH}}$ ,  $\Gamma_0^{\text{HH}}$ , and  $\sigma^{\text{HH}}$  obtained by fits to the PL spectra are also used to calculate the contribution from  $\mathcal{A}^{\text{HH}}(\hbar\omega)$ . For LH excitons,  $E^{\text{LH}}$ ,  $\Gamma_0^{\text{LH}}$ , and  $\sigma^{\text{LH}}$  are obtained from fits to the absorption spectra. The parameters  $\Gamma_c^J$  and  $E_X^J$  are also fitted, while  $\sigma_c^J$  is taken to be zero for simplicity, as we expect delocalized continuum states to be less affected by local disorder.

Figure 4 shows the obtained fits (thin black lines) and the experimental absorption (thick colored lines). The total contribution from HH (solid blue lines) and LH excitons (solid magenta lines) are also shown together with the corresponding continuum contributions (dashed lines). Thin colored lines depict different  $n$  states for HH excitons. Our model thus reproduces very well the entire absorption spectrum for different lateral sizes of NPLs. The fitting procedure results in exciton binding energies equal to  $E_X^{\text{HH}} = 135 \pm 2$  meV and  $E_X^{\text{LH}} = 301 \pm 4$  meV, which are independent of the lateral sizes to within the uncertainty. This is to be expected since  $L_x, L_y > a_B^{2D}$  for all samples and is consistent with our separable ansatz for the exciton wave functions on which our model is based. Other fitting parameters are listed in Table SMI of the Supplemental Material [28]. Note that all fit parameters do not depend on the lateral sizes of the NPLs, as expected. The asymmetry of the HH peak clearly depends on the presence of different exciton c.m. motional states. The (1,3) state redshifts on going from sample S5 to sample S1 due to the increase of the lateral size  $L_y$ . In addition, the enhanced HH asymmetry for sample S1 results from the similar contributions of (1,3) and (3,1) states. The slight disagreement on the high-energy side of the HH absorption peak is probably related to the contribution from internally excited excitons and their c.m. states, also seen from the emission spectra.

## VI. CONCLUSIONS

In conclusion, different from Ref. [15], we demonstrated that effects of the lateral size of CdSe NPLs on PL and

optical absorption spectra can be fully attributed only to the quantized exciton c.m. motion, which for the relatively weak confinement considered here can, in a good approximation, still be separated from their relative motion. In fact, for the NPL sizes investigated herein, the experimental spectra can be reproduced theoretically on the basis of the simple particle-in-a-box model for the translational motion of the exciton within a NPL. Importantly, it was not necessary to take into account size-dependent effects of phonons on PL and absorption spectra. Our results show that variation of the lateral size of (quasi-)two-dimensional materials provides a tool to tune their excitonic and therefore optoelectronic properties in addition to modifying the thickness. These insights also open the road to studying, with similar precision spectroscopy that resolves the c.m. energy levels as presented here, nontrivial quantum effects such as the Berry phase on the c.m. motion of topological excitons in NPLs consisting of topological insulator materials.

## ACKNOWLEDGMENTS

L.D.A.S. and M.F. thank A. W. Achtstein for the very helpful discussions. This work is part of the research program TOP-ECHO with Project No. 715.016.002, which is financed by the Netherlands Organization for Scientific Research (NWO).

- 
- [1] S. Ithurria and B. Dubertret, Quasi 2D colloidal CdSe platelets with thicknesses controlled at the atomic level, *J. Am. Chem. Soc.* **130**, 16504 (2008).
  - [2] J. Yu and R. Chen, Optical properties and applications of two-dimensional CdSe nanoplatelets, *InfoMat* **2**, 905 (2020).
  - [3] A. Naeem, F. Masia, S. Christodoulou, I. Moreels, P. Borri, and W. Langbein, Giant exciton oscillator strength and radiatively limited dephasing in two-dimensional platelets, *Phys. Rev. B* **91**, 121302(R) (2015).
  - [4] A. W. Achtstein, A. Schliwa, A. Prudnikau, M. Hardzei, M. V. Artemyev, C. Thomsen, and U. Woggon, Electronic structure and exciton-phonon interaction in two-dimensional colloidal CdSe nanosheets, *Nano Lett.* **12**, 3151 (2012).
  - [5] R. Tomar, A. Kulkarni, K. Chen, S. Singh, D. van Thourhout, J. M. Hodgkiss, L. D. A. Siebbeles, Z. Hens, and P. Geiregat, Charge carrier cooling bottleneck opens up nonexcitonic gain mechanisms in colloidal CdSe quantum wells, *J. Phys. Chem. C* **123**, 9640 (2019).
  - [6] A. W. Achtstein, O. Marquardt, R. Scott, M. Ibrahim, T. Riedl, A. V. Prudnikau, A. Antanovich, N. Owschimikow, J. K. N. Lindner, M. Artemyev, and U. Woggon, Impact of shell growth on recombination dynamics and exciton-phonon interaction in CdSe/CdS core-shell nanoplatelets, *ACS Nano* **12**, 9476 (2018).
  - [7] M. Li, M. Zhi, H. Zhu, W.-Y. Wu, Q.-H. Xu, M. H. Jhon, and Y. Chan, Ultralow-threshold multiphoton-pumped lasing from colloidal nanoplatelets in solution, *Nat. Commun.* **6**, 8513 (2015).
  - [8] R. Scott, A. W. Achtstein, A. Prudnikau, A. Antanovich, S. Christodoulou, I. Moreels, M. Artemyev, and U. Woggon, Two photon absorption in II-VI semiconductors: The influence of dimensionality and size, *Nano Lett.* **15**, 4985 (2015).
  - [9] J. Heckmann, R. Scott, A. V. Prudnikau, A. Antanovich, N. Owschimikow, M. Artemyev, J. I. Climente, U. Woggon, N. B. Grosse, and A. W. Achtstein, Directed two-photon absorption in CdSe nanoplatelets revealed by  $k$ -space spectroscopy, *Nano Lett.* **17**, 6321 (2017).
  - [10] J. Q. Grim, S. Christodoulou, F. Di Stasio, R. Krahne, R. Cingolani, L. Manna, and I. Moreels, Continuous-wave biexciton lasing at room temperature using solution-processed quantum wells, *Nat. Nanotechnol.* **9**, 891 (2014).
  - [11] Z. Yang, M. Pelton, I. Fedin, D. V. Talapin, and E. Waks, A room temperature continuous-wave nanolaser using colloidal quantum wells, *Nat. Commun.* **8**, 143 (2017).
  - [12] S. Ithurria, M. D. Tessier, B. Mahler, R. P. S. M. Lobo, B. Dubertret, and A. L. Efros, Colloidal nanoplatelets with two-dimensional electronic structure, *Nat. Mater.* **10**, 936 (2011).
  - [13] G. H. V. Bertrand, A. Polovitsyn, S. Christodoulou, A. H. Khan, and I. Moreels, Shape control of zincblende CdSe nanoplatelets, *Chem. Commun.* **52**, 11975 (2016).
  - [14] F. Rajadell, J. I. Climente, and J. Planelles, Excitons in core-only, core-shell and core-crown CdSe nanoplatelets: Interplay between in-plane electron-hole correlation, spatial confine-

- ment, and dielectric confinement, *Phys. Rev. B* **96**, 035307 (2017).
- [15] M. Richter, Nanoplatelets as material system between strong confinement and weak confinement, *Phys. Rev. Mater.* **1**, 016001 (2017).
- [16] S. Ithurria, G. Bousquet, and B. Dubertret, Continuous transition from 3D to 1D confinement observed during the formation of CdSe nanoplatelets, *J. Am. Chem. Soc.* **133**, 3070 (2011).
- [17] A. Yeltik, S. Delikanli, M. Olutas, Y. Kelestemur, B. Guzelturk, and H. V. Demir, Experimental determination of the absorption cross-section and molar extinction coefficient of colloidal CdSe nanoplatelets, *J. Phys. Chem. C* **119**, 26768 (2015).
- [18] C. She, I. Fedin, D. S. Dolzhenkov, P. D. Dahlberg, G. S. Engel, R. D. Schaller, and D. V. Talapin, Red, yellow, green, and blue amplified spontaneous emission and lasing using colloidal CdSe nanoplatelets, *ACS Nano* **9**, 9475 (2015).
- [19] M. Olutas, B. Guzelturk, Y. Kelestemur, A. Yeltik, S. Delikanli, and H. V. Demir, Lateral size-dependent spontaneous and stimulated emission properties in colloidal CdSe nanoplatelets, *ACS Nano* **9**, 5041 (2015).
- [20] Q. Li and T. Lian, Area- and thickness-dependent biexciton auger recombination in colloidal CdSe nanoplatelets: Breaking the “universal volume scaling law,” *Nano Lett.* **17**, 3152 (2017).
- [21] Q. Li and T. Lian, A model for optical gain in colloidal nanoplatelets, *Chem. Sci.* **9**, 728 (2018).
- [22] R. F. Schnabel, R. Zimmermann, D. Bimberg, H. Nickel, R. Lösch, and W. Schlapp, Influence of exciton localization on recombination line shapes:  $\text{In}_x\text{Ga}_{1-x}\text{As}/\text{GaAs}$  quantum wells as a model, *Phys. Rev. B* **46**, 9873 (1992).
- [23] A. W. Achtstein, R. Scott, S. Kickhöfel, S. T. Jagsch, S. Christodoulou, G. H. V. Bertrand, A. V. Prudnikau, A. Antanovich, M. Artemyev, I. Moreels, A. Schliwa, and U. Woggon, *p*-State Luminescence in CdSe Nanoplatelets: Role of Lateral Confinement and a Longitudinal Optical Phonon Bottleneck, *Phys. Rev. Lett.* **116**, 116802 (2016).
- [24] D. P. Morgan, C. J. A. Maddux, and D. F. Kelley, Transient absorption spectroscopy of CdSe nanoplatelets, *J. Phys. Chem. C* **122**, 23772 (2018).
- [25] R. Scott, A. V. Prudnikau, A. Antanovich, S. Christodoulou, T. Riedl, G. H. V. Bertrand, N. Owschimikow, J. K. N. Lindner, Z. Hens, I. Moreels, M. Artemyev, U. Woggon, and A. W. Achtstein, A comparative study demonstrates strong size tunability of carrier-phonon coupling in CdSe-based 2D and 0D nanocrystals, *Nanoscale* **11**, 3958 (2019).
- [26] J. F. Specht, R. Scott, M. Corona Castro, S. Christodoulou, G. H. V. Bertrand, A. V. Prudnikau, A. Antanovich, L. D. A. Siebbeles, N. Owschimikow, I. Moreels, M. Artemyev, U. Woggon, A. W. Achtstein, and M. Richter, Size-dependent exciton substructure in CdSe nanoplatelets and its relation to photoluminescence dynamics, *Nanoscale* **11**, 12230 (2019).
- [27] M. D. Tessier, L. Biadala, C. Bouet, S. Ithurria, B. Abecassis, and B. Dubertret, Phonon line emission revealed by self-assembly of colloidal nanoplatelets, *ACS Nano* **7**, 3332 (2013).
- [28] See Supplemental Material at <http://link.aps.org/supplemental/10.1103/PhysRevB.102.195405> for details of sample preparation, TEM analysis and statistics, and fitting parameters.
- [29] F. García Flórez, L. D. A. Siebbeles, and H. T. C. Stoof, Effects of two-dimensional material thickness and surrounding dielectric medium on coulomb interactions and excitons, *Phys. Rev. B* **102**, 125303 (2020).
- [30] M. D. Tessier, C. Javaux, I. Maksimovic, V. Lorient, and B. Dubertret, Spectroscopy of single CdSe nanoplatelets, *ACS Nano* **6**, 6751 (2012).
- [31] R. Zimmermann and E. Runge, Excitons in narrow quantum wells: Disorder localization and luminescence kinetics, *Phys. Status Solidi A* **164**, 511 (1997).
- [32] R. Benchamekh, N. A. Gippius, J. Even, M. O. Nestoklon, J.-M. Jancu, S. Ithurria, B. Dubertret, A. L. Efros, and P. Voisin, Tight-binding calculations of image-charge effects in colloidal nanoscale platelets of CdSe, *Phys. Rev. B* **89**, 035307 (2014).
- [33] H. Haug and S. W. Koch, *Quantum Theory of the Optical and Electronic Properties of Semiconductors*, 5th ed. (World Scientific, Singapore, 2009).